Spectroscopic study of Er-doped Ga₂Ge₅S₁₃ glass for mid-IR laser applications

EI EI BROWN, 1,* D ZACKERY D. FLEISCHMAN, 1 JASON MCKAY, 1 UWE HOMMERICH, 2 WITOLD PALOSZ, 3 SUDHIR TRIVEDI, 3 AND MARK DUBINSKII 1

Abstract: We present mid-IR spectroscopic characterization of the low-phonon chalcogenide glass, $Ga_2Ge_5S_{13}$ (GGS) doped with Er^{3+} ions. Under the excitation at ~800 nm, Er^{3+} :GGS exhibited broad mid-IR emission bands centered at ~2.7, ~3.5, and ~4.5 µm at room temperature. The emission lifetime of the $^4I_{9/2}$ level of Er^{3+} ions in GGS glass was found to be millisecondlong at room temperature. The measured fluorescence lifetimes were nearly independent of temperature, indicating negligibly small nonradiative decay rate for the $^4I_{9/2}$ state, as can be expected for a low-maximum-phonon energy host. The transition line-strengths, radiative lifetimes, fluorescence branching ratios were calculated by using the Judd-Ofelt method. The peak stimulated emission cross-section of the $^4I_{9/2} \rightarrow ^4I_{11/2}$ transition of Er^{3+} ion was determined to be ~0.10×10⁻²⁰ cm² at room temperature.

© 2022 Optica Publishing Group under the terms of the Optica Open Access Publishing Agreement

1. Introduction

A great number of rare-earth (RE) activated gain materials have been investigated in the development of new solid-state infrared (IR) sources for a variety of applications including laser remote sensing, environmental monitoring, molecular spectroscopy, free-space communications as well as medicine [1–28]. All material types are being considered, from crystals to ceramics and glasses, with focus on those RE³⁺ hosts with low maximum phonon energy. Table 1 shows some examples of laser operation in the mid-IR region from several RE doped crystals such as fluorides and chlorides, as well as chalcopyrite crystals, and chalcogenide glasses [3–15]. The latter (in Table 1) are of particular interest due to the recent demonstration of mid-infrared (mid-IR) gain and lasing from RE³⁺ (Tb³⁺, Pr³⁺, Ce³⁺) doped low-phonon chalcogenide glasses which has sparked further development of this class of materials for fiber laser applications [13–15].

Gallium-germanium (GaGe) based materials have emerged as promising chalcogenide glass hosts for mid-IR laser applications due to their favorable glass-forming ability, chemical and mechanical durability, as well as high rare earth ion solubility [13–15,21–30]. Compared to Arsenic (As) based compositions, GaGe chalcogenide glasses offer the added advantage of being non-toxic. Recent reports on RE³⁺ doped GaGe-based chalcogenide glasses demonstrated upper laser level lifetimes as long as 3 - 7 ms for mid-IR transitions between the levels with only ~2000cm⁻¹ spacing [13–15]. As seen from Table 1, many of the GaGe glasses studied thus far for mid-IR lasing have been Selenide (Se) compositions. However, sulfide glasses offer some benefits, such as a wider optical bandgap, which allows for pumping with well-developed high power laser diode sources (~800 nm, ~980 nm) without the detrimental effects of two-photon absorption. Moreover, the sulfide glasses have low phonon energies (~340 - 400 cm⁻¹) for mitigating nonradiative multi-phonon decay rates, a high refractive index allowing for increased

#451131 Journal © 2022 https://doi.org/10.1364/OME.451131

¹DEVCOM Army Research Laboratory, ATTN: FCDD-RLS-CL, 2800 Powder Mill Rd, Adelphi, MD 20783, INA

²Department of Physics, Hampton University, Olin Engineering Bldg, Rm 102, 268 Emancipation Dr., Hampton, VA 23668, USA

³ Brimrose Technology Corporation, 19 Loveton Cir, Sparks Glencoe, MD 21152, USA *eiei.brown.civ@army.mil

RE ³⁺ :Host	Crystals/Glasses	λ (μm)	Laser Transition	Phonon Energy (cm ⁻¹)	Ref.
Dy ³⁺ :YLF	crystal	4.3	$^{6}\mathrm{H}_{11/2} \rightarrow ^{6}\mathrm{H}_{13/2}$	~ 560	[3]
Er ³⁺ :KPb ₂ Cl ₅	crystal	4.5	$^{4}I_{9/2} \rightarrow ^{4}I_{11/2}$	~ 203	[4]
Dy ³⁺ :RPb ₂ Cl ₅	crystal	5.5	$^{6}\text{H}_{9/2}$ + $^{6}\text{F}_{11/2}$ \rightarrow $^{6}\text{H}_{11/2}$	~ 203	[5]
Dy ³⁺ :KPb ₂ Cl ₅	crystal	4.4	$^{6}\mathrm{H}_{11/2} \rightarrow ^{6}\mathrm{H}_{13/2}$	~ 203	[6]
Pr ³⁺ :LaCl ₃	crystal	5.2	3 F ₃ \rightarrow 3 H ₆	~ 210	[7]
Pr ^{3 +} LaCl ₃	crystal	7.2	$^3F_3 \rightarrow ^3F_2$	~ 210	[8]
Dy ³⁺ :CaGa ₂ S ₄	crystal	4.3 - 4.4	$^{6}\text{H}_{11/2} \rightarrow ^{6}\text{H}_{13/2}$	~ 350	[9]
Dy ³⁺ :PbGa ₂ S ₄	crystal	4.3 - 4.4	$^{6}\text{H}_{11/2} \rightarrow ^{6}\text{H}_{13/2}$	~ 350	[10]
Ho ³⁺ :YLF	crystal	3.9	$^{5}I_{5} \rightarrow {}^{5}I_{6}$ (cascade)	~ 560	[11]
Ho ³⁺ :InF ₃	glass	3.9	$^{5}I_{5} \rightarrow ^{5}I_{6}$	~ 509	[12]
Tb ³⁺ :Ge ₃₆ Ga ₅ Se ₅₉	glass	4.9 - 5.5	$^{7}\text{F}_{5} \rightarrow ^{7}\text{F}_{6}$	~ 350	[13]
Pr ³⁺ : Ge ₃₆ Ga ₅ Se ₅₉	glass	5.5-5.9	$^3H_5 \rightarrow ^3H_4$	~ 350	[14]
Ce ³⁺ :Ge ₂₀ Sb ₁₀ Ga ₅ Se ₆₅	glass	5.1–5.5	${}^{2}F_{7/2} \rightarrow {}^{2}F_{5/2}$	~ 350	[15]

Table 1. Recent demonstrations of mid-IR rare-earth lasers.

probability of spontaneous emissions, and a wide transmission window that extends well beyond $10\,\mu m$ [21–24]. Recent studies of various GaGe sulfide glasses have explored the effect of varying the Ga & Ge compositions [21–26], and among those studies, $Ga_2Ge_5S_{13}$ has emerged as one of the better candidates offering the cleanest Raman spectrum without the high-energy peaks observed in other compositions. Among RE^{3+} ions, Pr^{3+} , Tb^{3+} , Dy^{3+} , Ho^{3+} , and Er^{3+} , have a wide choice of energy levels with high potential for mid-IR transitions in the 3 - $5\,\mu m$ spectral range. In this work, we report the findings of our recent spectroscopic investigation of Er^{3+} doped $Ga_2Ge_5S_{13}$ (Er^{3+} :GGS) glass, including absorption and mid-IR emission studies The results of Judd-Ofelt analysis are also presented and discussed.

2. Experimental details

Er³+-doped GGS glasses were prepared using a standard "quench and anneal" procedure wherein a stoichiometric mixture of gallium (6N), germanium (6N), and sulphur (5N), and 1 - 2 wt.% of erbium (3N), were sealed in thin walled (1 mm) quartz ampoules with an inner diameter of 10 mm. The ampoule was sealed under high vacuum (better than 10^{-6} Torr) before being placed in a rocking furnace. The temperature of the ampoule was gradually increased to 920°C over a period of 5 days, while also being subjected to constant rocking. Then the ampoule was removed quickly from the furnace, quenched in cold water for a few seconds, and then put right back in the annealing furnace at 430°C. The furnace was gradually cooled over a period of 40 hours to room temperature. In this work, one undoped GGS glass and three Er³+ doped GGS glasses were explored. The Er³+ concentrations in the doped glasses were determined to be 0.975 wt.% $(1.61 \times 10^{20} \text{ cm}^{-3})$, 1.51 wt.% $(2.5 \times 10^{20} \text{ cm}^{-3})$, 2.09 wt.% $(3.46 \times 10^{20} \text{ cm}^{-3})$ using inductively coupled plasma optical emission spectroscopy (ICP-OES) by Galbraith Laboratories, Inc.

Room temperature transmission and absorption spectra were recorded using a Cary 6000i UV-Vis-NIR spectrophotometer and a Nicolet 6700 Fourier-transform infrared spectrometer. Mid-IR fluorescence spectra were excited by a continuous-wave Spectra-Physics Tsunami Ti:Sapphire laser. A Princeton Instruments Acton SpectraPro 0.15-m monochromator (λ_{blaze} : 4 µm, 150 grooves/mm) was used to acquire the mid-IR emission spectra. The emission signal was recorded by an Infrared Associates liquid-nitrogen-cooled InSb detector in conjunction with a Stanford Research Systems SR830 dual-phase lock-in amplifier. Fluorescence decay measurements were

carried out using the output of a pulsed (10-ns pulses, 10 Hz) Nd:YAG pumped Optical Parametric Oscillator system as an excitation source. The decay signal was recorded with a LabVIEW-driven National Instruments (USB-6366 DAQ) data acquisition system. For temperature-dependent emission studies down to 10 K, the sample was mounted on the cold finger of a two-stage closed-cycle CTI Cryodyne cryogenic refrigerator.

Raman spectra, used for assessing the maximum phonon energy of the glass, were measured in the range of $200\text{-}600\,\text{cm}^{-1}$ using a Renishaw InVia microscope equipped with 633 nm and 785 nm excitation sources. The Raman measurement result, performed on an undoped $Ga_2Ge_5S_{13}$ glass sample, is shown in Fig. 1. It shows the strongest phonon energy peak at $\sim 340\,\text{cm}^{-1}$, with the maximum phonon energy peak observed at $\sim 435\,\text{cm}^{-1}$. This result is in a good agreement with other reported Raman measurements performed on similar composition GGS glasses [27,28].

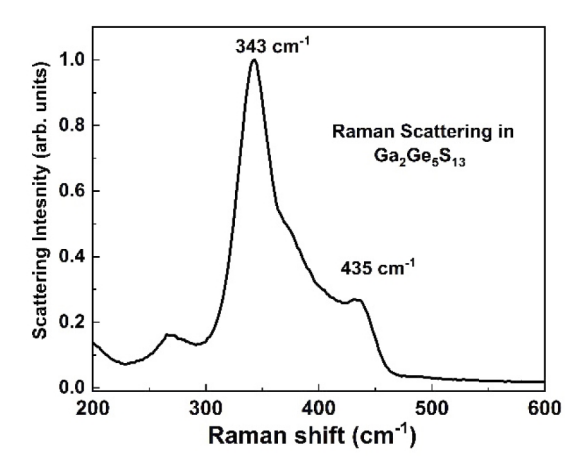


Fig. 1. Normalized Raman scattering spectrum of $Ga_2Ge_5S_{13}$ glass taken with a 633 nm excitation.

3. Results and discussion

3.1. Transmission, absorption and Judd-Ofelt analysis

Figure 2(a) shows the transmission spectra of undoped and 2wt.% Er^{3+} doped GGS glasses, and it can be noted that the fundamental absorption edge of GGS is located at ~ 480 nm. The undoped GGS glass registered a maximum background transmission of $\sim 80\%$, which is close to the limit defined by Fresnel reflections. The background transmission of the 2wt.% Er^{3+} :GGS glass is reduced to roughly 70%, most likely due to the incorporation of RE impurities, which decrease the overall optical transparency of the glass, likely due to defect formation. Several intra-4f Er^{3+} absorption bands are noticeable in the region from ~ 0.5 - $1.6\,\mu m$, providing evidence of the successful incorporation of Er^{3+} ions.

Figure 2(b) shows the absorption spectra of the undoped and 2wt.% $\rm Er^{3+}$ doped GGS glasses from 2 to 12 μm . The absorption for the doped glass has been vertically offset to accentuate the differences in the spectra. It is well known that sulphide glasses are prone to contamination caused by hydrogen and carbon impurities, which can lead to formation of the infrared absorption features [21–24]. It can be seen that both undoped and doped glasses showed several impurity absorption bands in the mid-IR region, related to $\rm CO_2$, $\rm COS$, $\rm H_2O$, $\rm OH$, and $\rm SH$ contaminants. The presence of these impurities indicates that the studied material is not fully optimized. Further improvements must be made to advance the material preparation, with emphasis on RE doping and the purification processes.

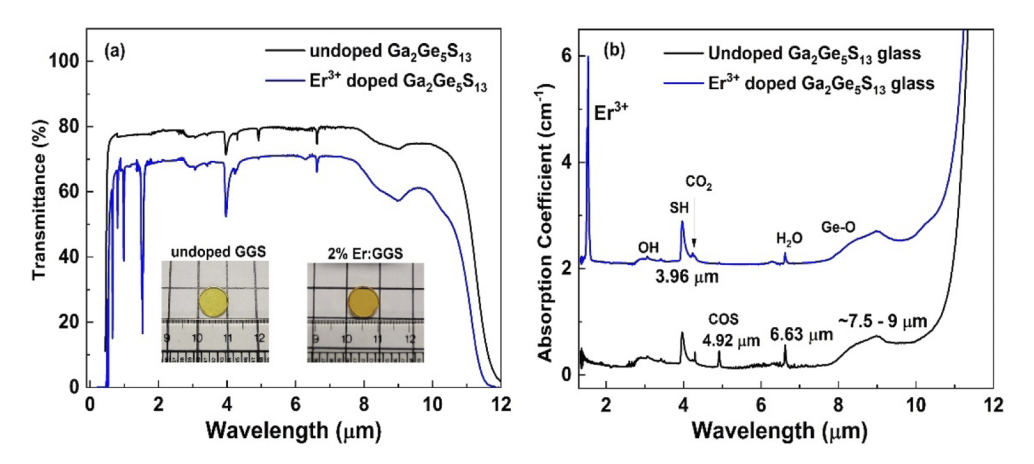


Fig. 2. Room temperature (a) transmission (images of undoped GGS and 2%Er:GGS glasses are shown) and (b) absorption spectra of undoped GGS (thickness: ~ 3.68 mm) and Er^{3+} doped GGS (thickness: ~ 3.77 mm) glasses. The absorption for the doped glass has been vertically offset to accentuate the differences in the spectra. The Er^{3+} concentration in this $Er^{3+}:GGS$ glass is determined to be 3.46×10^{20} cm⁻³. The hydrogen and carbon related impurity absorption bands are indicated.

The room temperature absorption coefficient spectrum of 2wt.% Er^{3+} :GGS is shown in Fig. 3(a), with assigned Er^{3+} intra-4f transitions originating from the ground state in the 0.4 to 1.8 μm region. The absorption spectrum was corrected for background losses due to Fresnel reflection and background loss. As indicated in Fig. 3(b), each Er^{3+} absorption band originates from the $^4I_{15/2}$ ground state and terminates at a higher excited state. The characteristic absorption bands of Er^{3+} were centered at $\sim\!1.532,\,0.985,\,0.810,\,0.662,\,0.549,\,0.528,\,\text{and}\,0.493\,\mu m$. It is well known that Er^{3+} have absorption bands at $\sim0.805\,\mu m\,(^4I_{15/2}\to^4I_{9/2})$ and $\sim0.983\,\mu m\,(^4I_{15/2}\to^4I_{11/2}),\,\text{which can be of great utility for laser diode pumping. These bands show peak absorption cross sections of <math display="inline">\sim\!0.24\times10^{-20}$ and 0.42×10^{-20} cm², respectively.

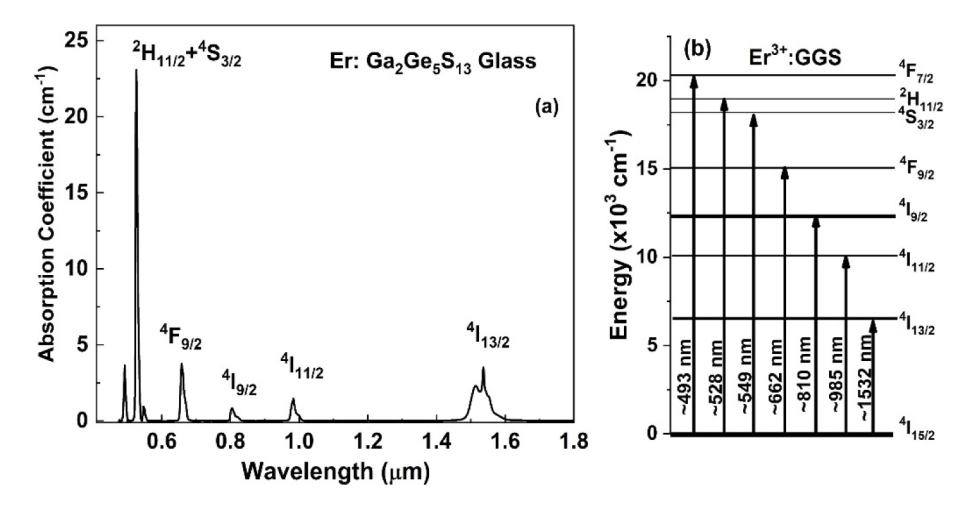


Fig. 3. (a) Room temperature absorption coefficient spectrum of Er^{3+} :GGS. The Er^{3+} concentration in this Er^{3+} :GGS glass is determined to be 3.46×10^{20} cm⁻³. (b) An energy level diagram indicating the absorption transitions corresponding to the absorption bands shown in the spectrum (a).

Six manifolds were selected to determine the three Ω_t parameters, known as the Judd-Ofelt (J-O) intensity parameters, for Er^{3+} transitions in GGS glass. The $^2H_{11/2}$ absorption band was not considered in the J-O analysis since it is known to be hypersensitive [1,31]. Table 2 shows the average Er^{3+} transition wavelengths, integrated absorption coefficients, and the line strengths for Er^{3+} :GGS glass. The significant magnetic dipole line strength component in the $^4I_{15/2} \rightarrow ^4I_{13/2}$ transition was subtracted from the corresponding experimental line strength value [1,31–34]. The magnetic transitions, which give negligible contribution to the Er^{3+} transition bands, are not considered in the present work. The measured and calculated line strength values are presented in the right column of the Table 2.

 S_{meas} (x 10^{-20} cm²) S_{calc} (x 10^{-20} cm²) Transitions Average $\int \alpha(\lambda) d\lambda \, (nm/cm)$ (from ⁴I_{15/2}) Wavelength (nm) $^{4}I_{13/2}$ 154.48 1531.75 1.467 1.557 $^{4}I_{11/2}$ 985.38 24.28 0.525 0.462 $^{4}I_{9/2}$ 810.07 14.003 0.368 0.389 $^{4}F_{9/2}$ 661.56 48.38 1.570 1.557 $^{4}S_{3/2}$ 549.24 7.11 0.276 0.187 $^{4}F_{7/2}$ 0.999 492.57 23.12 0.853

Table 2. Average transition wavelengths, integrated absorption coefficients and the line strengths of Er³⁺:Ga₂Ge₅S₁₃ glass.

The three J-O intensity parameters calculated from this analysis were $\Omega_2 = 4.51 \times 10^{-20}$ cm², $\Omega_4 = 2.20 \times 10^{-20}$ cm², and $\Omega_6 = 0.84 \times 10^{-20}$ cm². These J-O parameters are in reasonable agreement with reported values for other Er³⁺ doped sulphide glasses, examples of which are displayed in Table 3 with their respective Refs. [21,24,35]. The root mean square (rms) error between measured and calculated line strengths was calculated to be $\sim 0.19 \times 10^{-20}$ cm², which indicated good consistency between measured and calculated line strengths and is also comparable to rms values reported for other Er³⁺ doped glasses [21,24,35].

	•	•	. •	
Glasses	$\Omega_2 \ (\text{x} \ 10^{-20} \ \text{cm}^2)$	$\Omega_4 \ (x \ 10^{-20} \ cm^2)$	$\Omega_6 \ (\text{x} \ 10^{-20} \ \text{cm}^2)$	Reference
Er:Ga ₂ Ge ₅ S ₁₃	4.51	2.20	0.84	This work
Er:Ge ₂₈ Ga _{6.2} S _{65.3}	10.5	3.00	1.60	[24]
Er:Ge ₂₀ Ga ₅ Sb ₁₀ S ₆₅	8.70	2.50	1.40	[21]
Er:GaLaS	6.54	2.00	0.97	[35]

Table 3. Judd-Ofelt intensity parameters of Er³⁺ in sulphide glasses.

3.2. Emission and decay time studies

Figure 4(a) depicts the room temperature mid-IR emission bands of Er^{3+} :GGS in the wavelength ranges 2.4 –3.1 µm, 3.1–4.05 µm, 4.05–5.1 µm, which correspond to the ${}^4I_{11/2} \rightarrow {}^4I_{13/2}$, ${}^4F_{9/2} \rightarrow {}^4I_{9/2}$, and ${}^4I_{9/2} \rightarrow {}^4I_{11/2}$ transitions, respectively. Excitation of the upper levels of these transitions was attained by pumping at ~800 nm, which directly populated the ${}^4I_{9/2}$ level, and subsequently the ${}^4I_{11/2}$ level through radiative and nonradiative transitions. The ${}^4F_{9/2}$ level was excited using excitation at 660 nm. A schematic diagram of the relevant Er^{3+} energy levels indicating the excitation transitions and observed emission lines is shown in Fig. 4(b)). Mid-IR emissions centered at ~4.5, ~3.6, and ~2.7 µm were observed with spectral bandwidths of 0.32, 0.28, and 0.13 µm at full width at half maximum, respectively. All emissions showed broad spectral features, an indicator of inhomogeneous broadening typical for glass hosts [21,23,35,36]. Such broad features offer the possibility of wide wavelength tunability in these spectral bands.

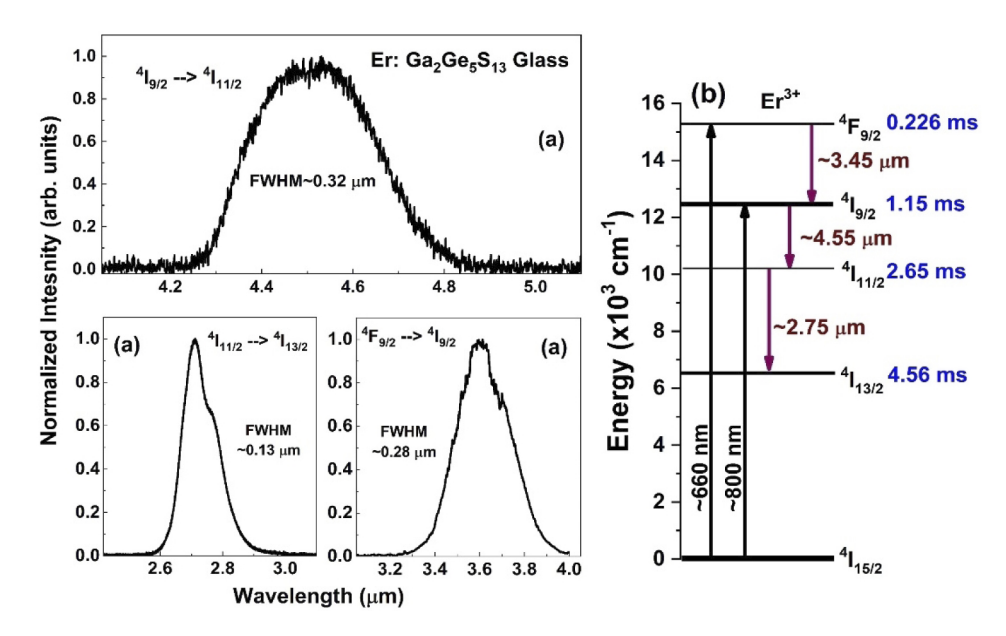


Fig. 4. (a) Room temperature normalized mid-IR emission spectra of ${}^4I_{9/2} \rightarrow {}^4I_{11/2}$, ${}^4I_{11/2} \rightarrow {}^4I_{13/2}$, and ${}^4F_{9/2} \rightarrow {}^4I_{9/2}$ transitions in Er³⁺:GGS glass. (b) The partial energy level diagram of Er³⁺ ions indicating the pump wavelength and corresponding emission transitions. The related emission lifetime values are listed on the right of each excited energy levels.

The emission lifetimes of the first four excited states of Er^{3+} :GGS glass were determined to be $\sim 4.56~\text{ms}~(^4I_{13/2}),~2.65~\text{ms}~(^4I_{11/2}),~1.15~\text{ms}~(^4I_{9/2}),~0.226~\text{ms}~(^4F_{9/2})$ at room temperature. These are longer lifetimes than those observed in other Er^{3+} doped sulphide glasses [21,35], particularly for the $^4I_{9/2}$ level which exhibits over a millisecond-long lifetime. Such long lifetimes reflect the lower maximum phonon energy of GGS glass, which leads to reduced nonradiative relaxation rates. There is an estimated $\sim 10\%$ error in reported decay times, attributed to inaccuracy in interpretation of the measured lifetime data.

In this work, the primary energy level of interest is ${}^4I_{9/2}$, which is the upper level of the 4.5 µm emission transition. The ${}^4I_{9/2}$ emission decay as a function of Er^{3+} concentration was performed to determine whether there was a change in lifetime (Fig. 5. (a)). We observed no significant quenching was up to 2wt.% Er^{3+} concentration. In order to rule out the possibilities that reabsorption was influencing the lifetime results, the pinhole method [37] was employed for during these lifetime measurements. Lengthening of the lifetimes due to reabsorption was found to be negligible. The decay transients were slightly non-exponential, which could possibly be due to energy transfer processes related to impurities (e.g. OH, SH) [21–24]. These processes should be negligible, however, due to the minimal overlap between SH absorption and Er^{3+} emission in the mid-IR region as shown in Fig. 5(b).

The observed long lifetimes have incited an interest in further exploration on temperature dependence of the spectral and decay dynamics. Figure 6(a) depicts the mid-IR emission spectra of the ${}^4I_{9/2} \rightarrow {}^4I_{11/2}$ transition for temperatures of 10, 77, 120, 200, and 295 K. The emission bandwidth of the studied Er^{3+} :GGS glass remained relatively broad, even at low temperatures, which can be favorable for tunable laser operation. Note the substantial red-shifting of the emission peak position with decreasing temperature, with a total shift of ~100 nm between the 10 K and 295 K. This shift can be attributed to the freezing out of the higher-lying Stark levels. Figure 6(b) depicts the ${}^4I_{9/2}$ emission lifetime as a function of temperature with the inset showing

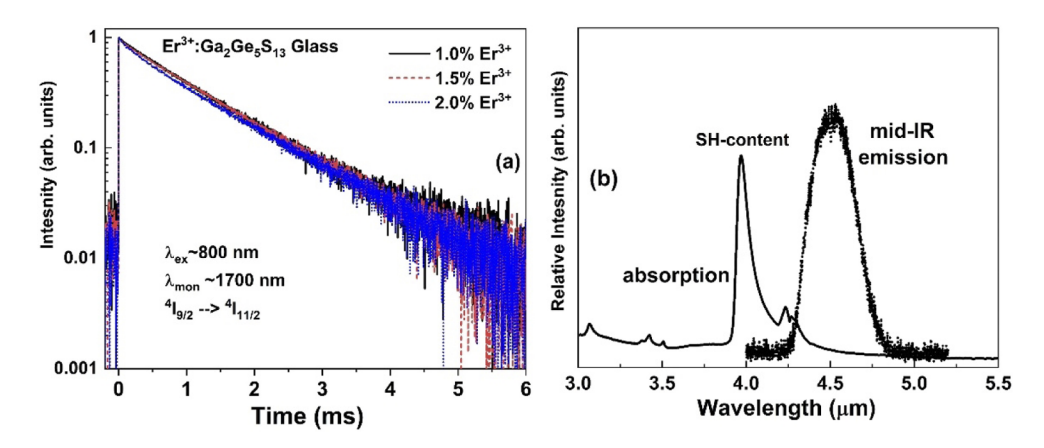


Fig. 5. (a) Room temperature decay transients of Er^{3+} ions at different concentrations of Er^{3+} in GGS glass, monitored at ~1700nm ($^4I_{9/2} \rightarrow ^4I_{13/2}$). (b) The spectral overlap between the SH-absorption and 4.5-µm emission in the mid-IR region.

the 77 K and 295 K decay curves of the ${}^4I_{9/2}$ level monitored at ${}^\sim1700$ nm (${}^4I_{9/2} \rightarrow {}^4I_{13/2}$). The measured ${}^4I_{9/2}$ lifetime is about a millisecond-long and no significant emission lifetime change was observed between 10 K and room temperature. This suggests that nonradiative processes due to a multi-phonon decay are negligible as expected from the energy-gap law for low phonon energy hosts [19,20].

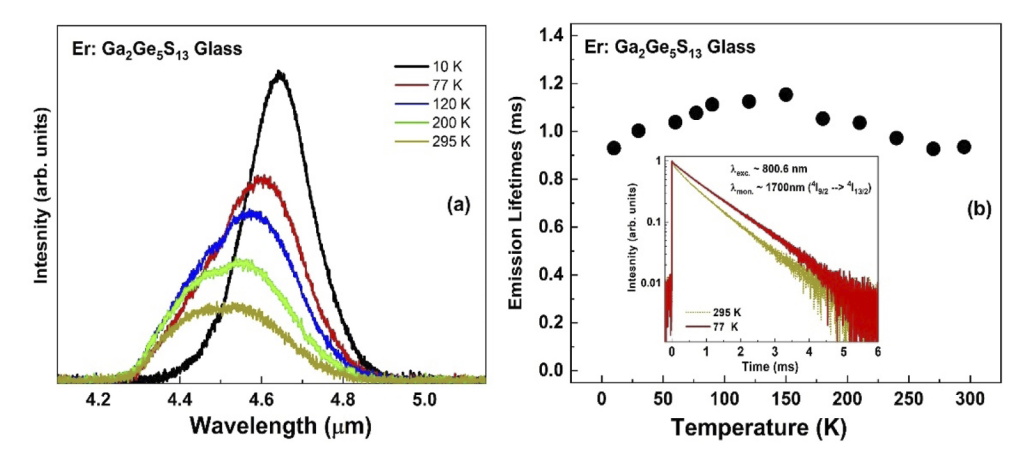


Fig. 6. (a) Temperature dependent mid-IR emission spectra of ${}^4I_{9/2} \rightarrow {}^4I_{11/2}$ transition. (b) The ${}^4I_{9/2}$ emission lifetimes as a function of temperature. The inset shows the emission decay of ${}^4I_{9/2}$ level at 77 K & 295 K.

Using the J-O parameters obtained for $\rm Er^{3+}$:GGS glass, the radiative transition rates, branching ratios, and radiative and measured lifetimes are presented in Table 4. The calculated radiative rates from the J-O analysis exhibit good agreement with measured rates for all four excited states, despite the estimated $\sim 10\%$ error for the radiative lifetimes calculated from the J-O analysis. This agreement is important because it confirms theoretically, what is seen in experiments: the excited states decay predominantly by the radiative route. The radiative emission lifetimes calculated from the investigated glass are comparable to the results obtained by others for $\rm Er^{3+}$

doped sulphide glasses [21,35]. The radiative lifetime estimated from J-O analysis is \sim 1.49 ms for the $^4I_{9/2}$ state, which leads to a radiative quantum efficiency of \sim 77% at room temperature.

Table 4. Er³⁺ transitions, average emission wavelengths, calculated radiative rates, branching ratios, radiative lifetimes (τ_{rad}) and measured lifetimes (τ_{exp}) of Er³⁺:Ga₂Ge₅S₁₃ glass.

Transitions	λ _{average} (nm)	A_{ij} (s ⁻¹)	β_{ij}	τ _{rad} (ms)	τ _{exp} (ms)
$^{4}I_{13/2} \rightarrow ^{4}I_{15/2}$	~1555	224.6	1	4.45	4.56
$^{4}I_{11/2} \rightarrow ^{4}I_{13/2}$	~2742	44.3	0.13	2.86	2.65
${}^{4}I_{11/2} \rightarrow {}^{4}I_{15/2}$	~986	305.1	0.87		
$^{4}I_{9/2} \rightarrow ^{4}I_{11/2}$	~4515	2.22	0.003	1.49	1.15
${}^{4}I_{9/2} \rightarrow {}^{4}I_{13/2}$	~1701	97.45	0.146		
${}^{4}I_{9/2} \rightarrow {}^{4}I_{15/2}$	~803	569.1	0.851		
${}^4F_{9/2} \rightarrow {}^4I_{9/2}$	~3499	10.84	0.002	0.216	0.226
${}^4F_{9/2} \rightarrow {}^4I_{11/2}$	~1970	141.71	0.031		
${}^4F_{9/2} \rightarrow {}^4I_{13/2}$	~1144	224.12	0.048		
${}^4F_{9/2} \rightarrow {}^4I_{15/2}$	~654	4256	0.919		

3.3. Stimulated emission cross-section

The stimulated emission cross section σ_{emiss} of the $^4I_{9/2} \rightarrow ^4I_{11/2}$ mid-IR transition (~4.5 µm) was calculated using the Füchtbauer-Ladenburg equation [38]:

$$\sigma_{emiss}(\lambda) = \frac{\beta \lambda^5 I(\lambda)}{8\pi n^2 c \tau_{rad} \int \lambda I(\lambda) d\lambda}$$
 (1)

where β and τ_{rad} are the branching ratio of the 4.5-µm emission (β = 0.003) and the radiative lifetime (τ_{rad} = 1.49 ms), respectively. $I(\lambda)$ is the emission intensity at wavelength λ and n is the refractive index of the host (n = 2.15). The emission cross-section spectra for Er³+:GGS glass is depicted in Fig. 7(a) for room temperature and 77 K, while Fig. 7(b) displays the partial energy level diagram of Er³+ ions indicating the emission transition of interest $^4I_{9/2} \rightarrow ^4I_{11/2}$. The peak emission cross section at \sim 4.52 µm was determined to be \sim 0.10 × 10⁻²⁰ cm² at room temperature whereas the value increased slightly for 77 K along with a shift to longer wavelengths. Table 5 shows the comparison of laser relevant parameters of Er³+ doped sulphide glasses. It was observed that the emission cross-section of the studied Er³+:GGS glass is smaller than the other sulphide glasses, mainly due to branching ratio of Er³+:GGS being one third of that of the others (see Table 5). Since branching ratio was determined theoretically via J-O analysis, further experimenting is required to experimentally determine the branching ratios of the transitions of interest for Er³+:GGS glass. Nonetheless, the sigma-tau (σ τ) product, which is typically characterized as a good figure of merit for lasers, compares well with the other Er³+ doped sulphide glasses.

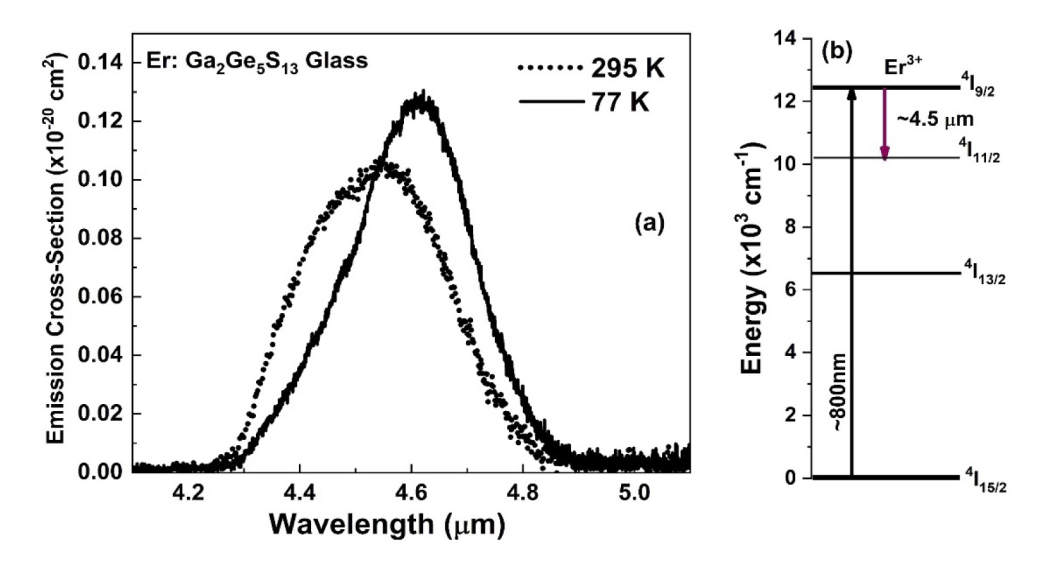


Fig. 7. (a) Emission cross-section spectrum for the ${}^4I_{9/2} \rightarrow {}^4I_{11/2}$ transition in Er^{3+} :GGS glass at room temperature and 77 K. (b) The partial energy level diagram of Er^{3+} ions indicating the excitation transition and the emission transition of interest ${}^4I_{9/2} \rightarrow {}^4I_{11/2}$.

Table 5. Branching ratios, radiative lifetimes (τ_{rad}) and measured lifetimes (τ_{exp}) , quantum efficiency (η_{QE}) , emission cross-sections (σ_{emiss}) , and sigma-tau $(\sigma\tau)$ product of the $^4I_{9/2}$ excited state for Er^{3+} : $Ga_2Ge_5S_{13}$ glass and other Er^{3+} doped sulphide glasses.

	RE:Glasses	λ _{peak} (μm)	β_{ij}	τ _{rad} (ms)	τ _{exp} (ms)	η _{QE} (%)	$\sigma_{emiss} (\lambda) \ (x10^{-20} \text{ cm}^{-1})$	στ (x10 ⁻²⁰ cm ⁻¹ .ms)
]	Er ³⁺ :Ga ₂ Ge ₅ S ₁₃	~4.52	0.003	1.49	1.15	~77	~0.10	0.115
Er ³	³⁺ :Ge ₂₀ Ga ₅ Sb ₁₀ S ₆₅	~4.60	0.008	1.10	0.70	~64	~0.28	0.196 [21]
	Er ³⁺ :GaLaS	~4.53	0.01	1.20	0.59	~50	~0.25	0.147 [35]

4. Conclusions

In summary, we have presented what is believed to be the first spectroscopic analysis of Er^{3+} doped $Ga_2Ge_5S_{13}$ glass, as it pertains to its potential for mid-IR lasing. The absorption spectrum of Er^{3+} :GGS glass displayed the characteristic Er^{3+} transitions in the visible and IR spectral region, which were used to perform Judd-Ofelt analysis. Optical excitation into the $^4I_{15/2} \rightarrow ^4I_{9/2}$ absorption band at ~ 800 nm resulted in observation of mid-IR Er^{3+} fluorescence bands, corresponding to the $^4I_{11/2} \rightarrow ^4I_{13/2}$ (~ 2.7 µm), and $^4I_{9/2} \rightarrow ^4I_{11/2}$ (~ 4.5 µm) transitions, respectively. The room temperature fluorescence lifetimes of the first four excited states of Er^{3+} :GGS glass were determined to be ~ 4.56 ms ($^4I_{13/2}$), 2.65 ms ($^4I_{11/2}$), 1.15 ms ($^4I_{9/2}$), and 0.226 ms ($^4F_{9/2}$). The emission decay of the $^4I_{9/2}$ level, which is of particular interest due to its being the upper level for the 4.5 µm emission, was nearly temperature independent. This observation is consistent with low-phonon energy hosts, despite the small energy gap (~ 2200 cm $^{-1}$) between the $^4I_{9/2}$ level and the next lower $^4I_{11/2}$ level. The peak mid-IR emission cross section of the $^4I_{9/2} \rightarrow ^4I_{11/2}$ transition at ~ 4.52 µm was determined to be $\sim 0.10 \times 10^{-20}$ cm 2 at room temperature. Overall, the promising spectral properties of the Er^{3+} doped $Ga_2Ge_5S_{13}$ glass make it an attractive gain material for mid-IR lasing.

Funding. National Science Foundation (NSF-DMR 1827820 (PREM)); Army Research Office (W911NF2120181, W911NF66020).

Acknowledgements. Brimrose Technology Corporation gratefully acknowledges the support of this work by Army Research Office through Cooperative Agreement W911NF2120181. The work at Hampton University was supported by the Army Research Office through Cooperative Agreement W911NF66020 and National Science Foundation through grant NSF-DMR 1827820 (PREM).

Disclosures. The authors declare no conflict of interest.

Data availability. Data underlying the results presented in this paper are not publicly available at this time but may be obtained from the authors upon reasonable request.

References

- 1. A.A. Kaminskii, Crystalline Lasers: Physical Processes and Operating Schemes (CRC Press, 1996).
- M. Eichhorn, "Quasi-three-level solid-state lasers in the near and mid infrared based on trivalent rare earth ions," Appl. Phys. B 93(2-3), 269–316 (2008).
- 3. N. P. Barnes and R. E. Allen, "Room temperature Dy:YLF laser operation at 4.34 μm," IEEE J. Quantum Electron. 27(2), 277–282 (1991).
- 4. S.R. Bowman, S.K. Searles, N.W. Jenkins, S.B. Qadri, E.F. Skelton, and J. Ganem, "Diode pumped room temperature mid-infrared erbium laser," in C Marshall, ed., *Advanced Solid-State Lasers*, OSA trends in optics and photonics, Vol. 50 (Optical Society of America, 2001), pp. 154–156.
- A. G. Okhrimchuk, L. N. Butvina, E. M. Dianov, I. A. Shestakova, N. V. Lichkova, V. N. Zagorodnev, and A. V. Shestakov, "Optical spectroscopy of the RbPb₂Cl₅:Dy³⁺ laser crystal and oscillation at 5.5 μm at room temperature," J. Opt. Soc. Am. B 24(10), 2690–2695 (2007).
- V. Savitski, P. Schlosser, L. Isaenko, and A. Tarasova, "Diode-pumped Dy:KPb₂Cl₅ laser at 4.2-4.45 μm," Laser Congress 2021 (ASSL, LAC) Optical Society of America, Paper number: ATu4A.1.
- S. R. Bowman, J. Ganem, B. J. Feldman, and A. W. Kueny, "Infrared laser characteristics of praseodymium-doped lanthanum trichloride," IEEE J. Quantum Electron. 30(12), 2925–2928 (1994).
- S. R. Bowman, L. B. Shaw, B. J. Feldman, and J. Ganem, "A 7-μm praseodymium-based solid-state laser," IEEE J. Quantum Electron. 32(4), 646–649 (1996).
- M.C. Nostrand, R.H. Page, S.A. Payne, and W.F. Krupke, "Room temperature CaGa₂S₄:Dy³⁺ laser action at 2.43 μm," in OSA TOPS in Optics and Photonics Series, Advanced Solid State Lasers, 26, 441–449 (1999).
- T.T. Basiev, M. E. Doroshenko, V. V. Osiko, and D. V. Badikov, "Mid IR laser oscillations in new low phonon PbGa₂S₄:Dy³⁺ crystal," *Technical Digest of OSA Topical Meetings*, Advanced Solid State Photonics (2005) paper TuB10, pp. 75–79.
- L. Esterowitz, R. C. Eckardt, and R. E. Allen, "Long-wavelength stimulated emission via cascade laser action in Ho:YLF," Appl. Phys. Lett. 35(3), 236–239 (1979).
- A. Berrou, C. Kieleck, and M. Eichhorn, "Mid-infrared lasing from Ho³⁺ in bulk InF₃ glass," Opt. Lett. 40(8), 1699–1701 (2015).
- 13. M. F. Churbanov, B. I. Denker, B. I. Galagan, V. V. Koltashev, V. G. Plotnichenko, M. V. Sukhanov, S. E. Sverchkov, and A. P. Velmuzhov, "First demonstration of ~5 (m laser action in terbium-doped selenide glass," Appl. Phys. B **126**(7), 117 (2020).
- 14. M. F. Churbanov, B. I. Denker, B. I. Galagan, V. V. Koltashev, V. G. Plotnichenko, G. E. Snopatin, M. V. Sukhanov, S. E. Sverchkov, and A. P. Velmuzhov, "Laser potential of Pr³⁺ doped chalcogenide glass in 5-6 (m spectral range," J. Non-Crys. Solids 559, 120592 (2021).
- B. I. Denker, B. I. Galagan, S. E. Sverchkov, V. V. Koltashev, V. G. Plotnichenko, M. V. Sukhanov, A. P. Velmuzhov, M. P. Frolov, Y. V. Korostelin, V. I. Kozlovsky, S. O. Leonov, P. Fjodorow, and Y. K. Skasyrsky, "Resonantly pumped Ce³⁺ mid-infrared lasing in selenide glass," Opt. Lett. 46(16), 4002–4004 (2021).
- L. D. Merkle, Z. Fleischman, E. Brown, J. L. Allen, U. Hommerich, and M. Dubinskii, "Enhanced mid-infrared emission of Pr³⁺ ions in solids through a "3-for-1" excitation process – quantified," Opt. Express 29(24), 39001–39015 (2021).
- E. Brown, Z. Fleischman, L. D. Merkle, E. Rowe, A. Burger, S. A. Payne, and M. Dubinskii, "Optical spectroscopy of holmium doped K₂LaCl₅," J Lumin. 196, 221–226 (2018).
- E. Brown, Z. Fleischman, J. McKay, and M. Dubinskii, "Spectroscopic characterization of low-phonon Er-doped BaF₂ single crystal for mid-IR lasers," Opt. Mater. Express 11(2), 575–584 (2021).
- M. Velazquez, A. Ferrier, J.-L. Doualan, and R. Moncorge, "Rare-earth doped low phonon energy halide crystals for mid-infrared sources," in A. Al-Khursan, ed., Solid-State Laser (IntechOpen, 2012), pp. 119–142.
- L. Isaenko, A. Yelisseyev, A. Tkachuk, and S. Ivanova, "New Monocrystals with Low Phonon Energy for Mid-IR Lasers," in M. Ebrahim-Zadeh and I. T. Sorokina Eds., Mid-Infrared Coherent Sources and Applications (Springer, 2008), pp. 3–65.
- V. Moizan, V. Nazabal, J. Troles, P. Houizot, J.-L. Adam, J.-L. Doualan, R. Moncorge, F. Smektala, G. Gadret, S. Pitois, and G. Canat, "Er³⁺-doped GeGaSbS glasses for mid-IR fiber laser application: Systhesis and rare earth spectroscopy," Opt. Mater. 31(1), 39–46 (2008).
- R. S. Quimby and B. G. Aitken, "Multiphonon energy gap law in rare-earth doped chalcogenide glass," J. Non-Cryst. Solids 320(1-3), 100–112 (2003).

1637

Optical Materials EXPRESS

- D. J. Coleman, P. Golding, and T. A. King, "Spectroscopic and energy-transfer parameters for Er³⁺-doped and Er³⁺, Pr³⁺-codoped GeGaS glasses," J. Opt. Soc. Am. B 19(9), 1982–1989 (2002).
- S. Kasap, K. Koughia, G. Soundararajan, and M. G. Brik, "Optical and photoluminescence properties of erbium-doped chalcogenide glasses (GeGaS:Er)," IEEE J. Sel. Top. Quantum Electron. 14(5), 1353–1360 (2008).
- V. S. Shiryaev and M. F. Churbanov, "Recent advances in preparation of high-purity chalcogenide glasses for mid-IR photonics," J. Non-Cryst. Solids 475, 1–9 (2017).
- M. Li, Y. Xu, X. Jia, L. Yang, N. Long, Z. Liu, and S. Dai, "Mid-infrared emission properties of Pr³⁺-doped Ge-Sb-Se-Ga-I chalcogenide glasses," Opt. Mater. Express 8(4), 992–1000 (2018).
- Y. Ledemi, S. H. Messaddeq, I. Skhripachev, S. J. L. Ribeiro, and Y. Messaddeq, "Influence of Ga incorporation on photoinduced phenomena in Ge-S based glasses," J. Non-Cryst. Solids 355(37-42), 1884–1889 (2009).
- S. H. Messaddeq, M. S. Liu, D. Lezal, Y. Messaddeq, S. J. L. Ribeiro, L. F. C. Oliveira, and J. M. D. A. Rollo, "Raman investigation of structural photoinduced irreversible changes of Ga₁₀Ge₂₅S₆₅ chalcogenide glasses," J. Optoelec. Ad. Mater. 3, 295–302 (2001).
- V. Nazabal, F. Starecki, J.-L. Doualan, P. Nemec, P. Camy, H. Lhermite, L. Bodiou, M.L. Anne, J. Carrier, and J.L. Adam, "Luminescence at 2.8 μm: Er³⁺-doped chalcogenide micro-waveguide," Opt. Mater. 58, 390–397 (2016).
- G. Louvet, S. Normani, L. Bodiou, J. Gutwirth, J. Lemaitre, P. Pirasteh, J.-L. Doualan, A. Benardais, Y. Ledemi, Y. Messaddeq, P. Nemec, J. Carrier, and V. Nazabal, "Co-sputtered Pr³⁺ doped Ga-Ge-Sb-Se active waveguides for mid-infrared operation," Opt. Express 28(15), 22511–22523 (2020).
- B.M. Walsh, "Judd-Ofelt theory: Principles and Practices," in B. Di Bartolo and O. Forte, Advances in Spectroscopy for Lasers and Sensing (Springer, 2006), pp. 403

 –433.
- 32. B. R. Judd, "Optical absorption intensities of rare-earth ions," Phys. Rev. 127(3), 750-761 (1962).
- 33. G. F. Ofelt, "Intensities of crystal spectra of rare-earth ions," J. Chem. Phys. 37(3), 511–520 (1962).
- W. T. Carnall, P. R. Fields, and K. Rajnak, "Spectral intensities of the trivalent lanthanides and actinides in solution. II," J. Chem. Phys. 49(10), 4412–4423 (1968).
- C. C. Ye, D. W. Hewak, M. Hempstead, B. N. Samson, and D. N. Payne, "Spectral properties of Er³⁺-doped gallium lanthanum sulphide glass," J. Non-Cryst. Solids 208(1-2), 56–63 (1996).
- 36. T. Schweizer, D. J. Brady, and D. W. Hewak, "Fabrication and spectroscopy of erbium doped gallium lanthanum sulphide glass fibers for mid-infrared laser applications," Opt. Express 1(4), 102–107 (1997).
- H. Kühn, S. T. Fredrich-Thornton, C. Kränkel, R. Peters, and K. Petermann, "Model for the calculation of radiation trapping and description of the pinhole method," Opt. Lett. 32(13), 1908–1910 (2007).
- B. F. Aull and H. P. Jenssen, "Vibronic interactions in Nd:YAG resulting in nonreciprocity of absorption and stimulated emission cross sections," IEEE J. Quantum Electron. 18(5), 925–930 (1982).